International Journal of Fracture **64**: 221–237, 1993.

Asymptotic analysis of a cohesive crack: 2. Influence of the softening curve

J. PLANAS and M. ELICES
Departamento de Ciencia de Materiales, Escuela de Ingenieros de Caminos, Universidad Politécnica de Madrid, 28040-Madrid, Spain

Received 15 June 1993; accepted in final form 31 August 1993

Abstract. This paper presents a numerical method well suited to solve the integral equation governing the asymptotic behavior of a cohesive crack, and uses it to analyze the influence of the softening curve on the cracking response of large specimens. The analysis is performed with two main objectives in mind: (1) providing criteria to determine when a simplified linear elastic fracture mechanics (LEFM) approach can be applied, and (2) providing possible procedures of extracting information on the softening behavior from experimental data. The main conclusion is that the effective crack extension prior to peak is nearly determined by the length of the softening curve (the critical crack opening) and so is the deviation from LEFM. Furthermore, a simplified $\mathcal{R}$-curve approach is proposed as an approximate alternative to solving the governing integral equation.

1. Introduction

When a crack is created in a material such as concrete, rock, or a ceramic, generically called *quasi-brittle* materials, a situation develops whereby the crack extends and its faces become bridged by unbroken ligaments whose average behavior may be represented by a decreasing stress versus crack opening relationship. In this sense the material may be said to *soften* and the softening region may be modeled by a *cohesive* zone, coplanar with the crack, where the restraining – or *cohesive* – stresses reflect the softening behavior of the material under consideration. The initial models of Barenblatt and Dugdale [1, 2] in the early sixties – dealing with different physical problems but formally similar – were generalized and applied to concrete by Hillerborg [3, 4] and are a current research topic in ceramics [5, 6].

Despite their apparently brittle behavior, it is well known that the linear elastic fracture mechanics (LEFM) approach is not applicable, in general, to quasi-brittle (cohesive) materials, so the analysis of the fracture behavior of these materials requires more involved techniques. On the other hand, it has been established that for *large sizes* both approaches must coincide and hence LEFM can be applied if the size of the specimen, or of the cracked structure, is *large enough.*

It is not an easy task to ascertain when the size is large enough for LEFM to apply; this size is different for ceramic materials, for rocks, and for cementitious composites and these *large* sizes may span several orders of magnitude depending on the characteristics of the softening curve, particularly on its shape. The essential aim of this paper is to investigate the influence of the softening curve in the deviations of quasi-brittle materials from LEFM in the limit of large sizes using a special semi-analytical procedure developed in previous work [7, 8, 9]. The research includes the analysis of other aspects which also depend on the softening curve and may help in ascertaining the suitability of different softening models when analyzing experimental results: The shape of the displacement field near the crack tip, and the specimen compliance among others.

This paper is structured as follows: Section 2 reviews some analytical results for cohesive cracks when the specimen size D is *large* ($D/R \gg 1$, where R is the cohesive zone size). Section 3 includes the description of the numerical procedures and the analysis of their performances. In Section 4 the influence of the softening functions on the stress and displacement fields near the cohesive crack is considered in detail, as well as the far fields and the connection with the far fields of an equivalent linear elastic sample. Finally, Section 5 discusses some practical aspects: How large the size must be for LEFM to hold within given bounds, and how to make an estimate of the evolution of the remote fields without recourse to numerical procedures.

2. Asymptotic analysis: Summary of previous results

We face the problem of mode I loading of a specimen with a characteristic dimension (a size, for short) D and assume that the fracturing behavior is well described by a cohesive crack model. In these conditions, a cohesive crack grows ahead of the initial crack tip as shown in Fig. 1a. The size of the cohesive zone is denoted as R and is taken as the independent variable in the following analysis.

The cohesive crack model is defined by the *softening curve*, the equation relating the stress transferred across the cohesive crack faces σ, to the crack opening displacement w

$$\sigma = F(w), \tag{1}$$

where $F(w)$ is a non-increasing, non-negative function defined for positive crack openings, as depicted in Fig. 1b. The area enclosed by the curve and the coordinate axes is the *fracture energy* G_F.

In the remainder of this section we include a summary of the relevant results previously obtained by the authors in [8]. The cohesive crack problem was formulated as a weighted superposition of solutions of auxiliary linear elastic fracture mechanics problems and was reduced to solving a functional integral equation. The asymptotic analysis is then performed by expanding the functions appearing in the integral equation in powers of R/D (the relative size of the cohesive zone), an asymptotically vanishing variable. It immediately turns out that when the series is truncated to $N + 1$ terms (where N is the order of the approximation) the previous functional equation splits into $N + 1$ integral equations which allow calculation of the $N + 1$ coefficients of the truncated series. In this paper we restrict our attention to the zero order approximation, and so we restrict the background exposition to this limiting case.

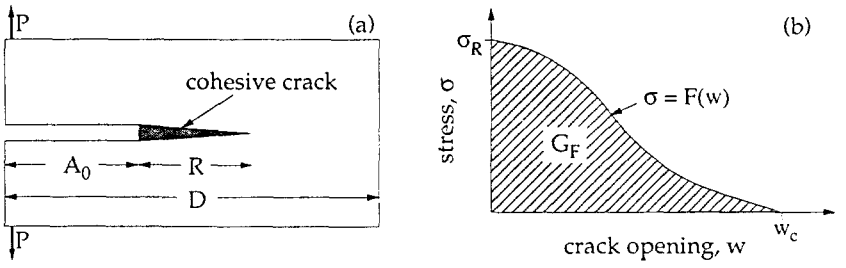

Fig. 1. (a) Cohesive crack in mode I. (b) General softening curve.

2.1. Notation and definitions

We follow [8] and denote all linear dimensions of the specimen and coordinates by upper case Latin letters, as shown in Fig. 2. In particular D is the size of the specimen, B its thickness, A_0 the initial crack length, R the cohesive zone extent, and C denotes the length of an ideal elastic crack. Other distances to characteristic points are shown in Fig. 2.

In [8], linear dimensions relative to size D were extensively used and were represented by lower case Latin letters. In the present case, where the order zero is analyzed, the only relevant relative dimensions are the relative initial crack length a_0, the relative cohesive zone size r, and the relative depth of an ideal crack length c, which are defined as

$$a = \frac{A}{D}, \quad r = \frac{R}{D}, \quad c = \frac{C}{D}. \tag{2}$$

For the asymptotic analysis, the only relevant dimension is that of the cohesive zone, and the set of reduced variables relative to R are denoted by lower case Greek letters. In particular ξ and ζ denote positions relative to the cohesive zone. Referring to Fig. 2, the corresponding reduced variables are

$$\xi = \frac{X}{R}, \quad \zeta = \frac{T}{R}. \tag{3}$$

The load acting upon the specimen is better described using the stress intensity factor for an ideal crack. For a crack of arbitrary relative length c, the stress intensity factor may be written as

$$K_I = \sigma_N \beta_0(c)\sqrt{2\pi D}, \tag{4}$$

where σ_N is a nominal stress proportional to P/BD, P being the applied load, and $\beta_0(c)$ a non-dimensional shape function.

The *nominal* stress intensity factor is used in the following as a measure of the load acting on the cohesive specimen. It is defined as the value of the stress intensity factor computed for the actual load and the initial crack length, i.e.

$$K_{IN} = \sigma_N \beta_0(a_0)\sqrt{2\pi D} = \sigma_N \beta_{00}\sqrt{2\pi D}. \tag{5}$$

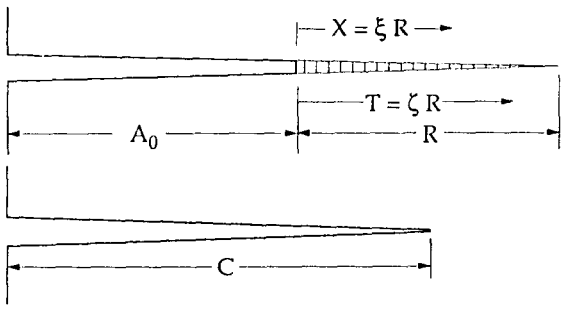

Fig. 2. Notation used for the cohesive crack problem and the auxiliary non-cohesive crack.

The results are presented in dimensionless form (represented by starred characters) using various combinations of the material properties σ_R, G_F and E' (generalized elastic modulus, $E' = E$ for plane stress, $E' = E/(1 - \nu^2)$ for plane strain, ν = Poisson's ratio). In particular, stresses, crack openings, and cohesive crack lengths take the following dimensionless forms

$$\sigma^* = \frac{\sigma}{\sigma_R}, \quad w^* = \frac{w}{w_{ch}}, \quad R^* = \frac{R}{l_{ch}}, \tag{6}$$

where the *characteristic crack opening* w_{ch} and the *characteristic length* l_{ch} are defined as

$$w_{ch} = \frac{G_F}{\sigma_R}, \quad l_{ch} = \frac{G_F E'}{\sigma_R^2}. \tag{7}$$

The dimensionless version of the softening function is written as

$$\sigma^* = F^*(w^*), \tag{8}$$

where $F^*(w^*)$ is related to $F(w)$ in (1) by $F^*(w^*) = F(w^* w_{ch})/\sigma_R$.

2.2. *The basic equation for the zeroth order asymptotic approach*

The main result of the asymptotic analysis performed in [8] is that the solution of the zero order approximation (valid for $R/D \ll 1$) may be written in terms of a single scalar dimensionless function $p_0(\xi)$ defined over [0, 1]. But it turns out that p_0 appears always in the combination $\beta_{00} p_0$. Therefore, in the following we write $k^*(\xi) = \beta_{00} p_0(\xi)$, as in [9]. With this notation, the integral equation to be solved for $k^*(\xi)$ is

$$\int_0^\xi (\xi - \zeta)^{-1/2} k^*(\zeta)\, \mathrm{d}\zeta = F^*\left[8R^* \int_\xi^1 (\zeta - \xi)^{1/2} k^*(\zeta)\, \mathrm{d}\zeta \right]. \tag{9}$$

As already pointed out, R^* is the independent variable, and it must be understood that the solution for $k^*(\zeta)$ depends on it. The solution depends on the material properties through the softening curve $F^*(w^*)$.

In the foregoing equation, the left hand member represents the stress distribution over the cohesive zone. Likewise, the bracketed expression in the right hand member is the crack opening distribution along the cohesive zone.

An essential aspect to consider for numerical formulations is the possibility of singular behavior of the unknown function $k^*(\zeta)$. This may be detected by writing that the left hand side of (9) is equal to the cohesive stress distribution

$$\int_0^\xi (\xi - \zeta)^{-1/2} k^*(\zeta)\, \mathrm{d}\zeta = \sigma_{\mathrm{coh}}(\xi). \tag{10}$$

This Volterra-type integral equation may be inverted [8, 9] to give

$$k^*(\zeta) = \frac{\sigma_{\mathrm{coh}}(0^+)}{\pi\sqrt{\zeta}} + \frac{1}{\pi} \int_0^\zeta (\zeta - \xi)^{-1/2} \frac{\mathrm{d}\sigma_{\mathrm{coh}}(\xi)}{\mathrm{d}\xi}\, \mathrm{d}\xi, \tag{11}$$

which shows that $k^*(\zeta)$ displays a $\zeta^{-1/2}$ singularity whenever there is a stress discontinuity at the initial crack tip ($\sigma_{coh}(0^+) \neq 0$).

2.3. Expressions for the nominal stress intensity factor and the near-tip fields

Once the density function $k^*(\xi)$ is obtained from (9), the dimensionless nominal stress intensity factor K_{IN}^* is given by

$$K_{IN}^* = \frac{K_{IN}}{\sqrt{EG_F}} = \sqrt{2\pi R^*} \int_0^1 k^*(\zeta)\, d\zeta. \tag{12}$$

The stress and crack opening fields on and *near* the cohesive zone are given by [8]

$$\sigma^*(\xi) = \int_0^1 (\xi - \zeta)^{-1/2} k^*(\zeta) H(\xi - \zeta)\, d\zeta, \tag{13}$$

$$w^*(\xi) = 8R^* \int_0^1 (\zeta - \xi)^{-1/2} k^*(\zeta) H(\zeta - \xi)\, d\zeta, \tag{14}$$

where $H(\eta)$ is the Heaviside step distribution.

2.4. Far-fields and effective crack extension

The fields far from the cohesive zone cannot be computed using the foregoing expressions, because those require that $\xi = X/R \ll D/R$. The expressions valid for far-field expressions were discussed in [8] and an essential theorem was proved regarding the far-field distribution. This theorem reads as follows:

For a cohesive material and a general geometry under proportional mode I loading, every-far field may be approximated, up to order R/D, by the far-field corresponding to an equivalent elastic crack of length $A_0 + \Delta A_\infty$, subjected to the same load. The far field equivalent extension ΔA_∞ is given by

$$\Delta A_\infty = R\langle\zeta\rangle, \tag{15}$$

where subscript ∞ indicates that this corresponds to the large size approximation, and $\langle\zeta\rangle$ is the k-average of ζ over the fracture process zone, i.e. the position of the center of gravity of the k distribution

$$\langle\zeta\rangle = \frac{\int_0^1 \zeta k^*(\zeta)\, d\zeta}{\int_0^1 k^*(\zeta)\, d\zeta}. \tag{16}$$

2.5. Lower bound theorems

The deviation from LEFM in the large size limit is controlled by the effective crack extension. In general it is not possible to find a closed form expression for it, and one has to solve (9) numerically to get the value of ΔA_∞. However, a closed form lower bound can be found in terms

of the material properties and the crack tip opening displacement (CTOD) [8, 9]. The lower bound theorems state that

$$R^* \geqslant \frac{\Delta A_\infty}{l_{ch}} \geqslant \tfrac{1}{32}\pi \frac{\mathrm{CTOD}^{*2}}{W_F^*}, \tag{17}$$

where $W_F^*(\mathrm{CTOD}) = W_F(\mathrm{CTOD})/G_F$ and

$$W_F(\mathrm{CTOD}) \equiv W_F[w(0)] = \int_0^{w(0)} F(w')\,\mathrm{d}w'. \tag{18}$$

In particular, when the CTOD reaches the critical crack opening value w_c, the critical cohesive zone size and effective crack extension verify

$$R_c^* \geqslant \frac{\Delta A_{\infty c}}{l_{ch}} \geqslant \tfrac{1}{32}\pi(w_c^{*2}). \tag{19}$$

2.6. Asymptotic size effect

The far field property just summarized is at the base of the determination of the asymptotic size effect curve [8, 9]. The result is that the effect of the size D on the apparent toughness, K_{INmax} may be written in the form

$$\frac{E'G_F}{K_{\mathrm{INmax}}^2} = 1 + 2\frac{\beta_{01}}{\beta_{00}}\frac{\Delta A_{\infty c}}{D}, \tag{20}$$

where $\Delta A_{\infty c}$ is the critical effective crack extension (we call *critical* the situation where the strength at the initial crack tip has been exhausted, i.e.: when $\sigma(0^+) = 0$ or $w(0) = \mathrm{CTOD} = w_c$). The factor β_{01} is related to the geometric shape factor $\beta_0(c)$ in (4) by

$$\beta_{01} = \left.\frac{\mathrm{d}\beta_0(c)}{\mathrm{d}c}\right|_{c=a_0}. \tag{21}$$

3. Numerical methods

Analytical solutions for the integral equation (9) are scarce. To the authors' knowledge, the only complete analytical solutions available correspond to rectangular softening (Dugdale type), and to softening functions built of rectangular blocks, in which cases the inversion formula (11) reduces the problem to a set of algebraic equations. The piece-wise rectangular softening functions have been extensively explored by Smith [10]. In particular Smith analyzed an extreme case of a two-step softening function in which the first step may be approximated by a Dirac δ-distribution, which leads to relatively compact solutions and may give a good representation of brittle matrix composite materials.

A partial analytical solution may be obtained by assuming a priori the shape of the spatial distribution of stress, or the spatial distribution of crack opening displacement along the cohesive zone *in the critical situation.* In this method, the softening function is obtained as an output of the analysis. Smith [11] investigated the case where the critical crack opening distribution is a linear combination of power laws of the type $1 - \xi^{(n+3/2)}$ $(n = 0, 1, \ldots)$, and obtained expressions for the length of the critical cohesive zone as a function of the critical crack opening [11].

For any other softening one has to resort to numerical methods to solve the integral equation. This is the topic of this section.

3.1. Interpolating functions and equation discretization

Since this is a very particular problem, particular methods of solution were envisaged. The most obvious one was to use global polynomial shape functions and point collocation (on a number of properly selected nodal points). This was so because the required integrals were easily expressible analytically (in terms of the Eulerian Γ function). The results were very good for a small number of terms, but started to show ill-behaved trends for polynomial degrees over 20.

Therefore, piecewise interpolating shape functions are used in a formulation very similar to finite elements. To get maximum simplicity, collocation at the nodes is used so that the following discrete set of equations is obtained

$$L_{ij} g_j = F^*(R^* U_{ij} g_j), \quad i, j = 1, 2, \ldots, N, \tag{22}$$

where g_j is the jth nodal value of $g(\zeta)$, L_{ij} is a constant lower triangular matrix, U_{ij} a constant upper triangular matrix, and N the number of nodes of the mesh. Repeated indices imply summation.

The elements of the matrices are given by

$$L_{ij} = \int_0^{\xi_i} \zeta^{-1/2} (\xi_i - \zeta)^{-1/2} \phi_j(\zeta) H(\xi_i - \zeta)\, \mathrm{d}\zeta, \tag{23}$$

$$U_{ij} = 8 \int_{\xi_i}^{1} \zeta^{-1/2} (\zeta - \xi_i)^{-1/2} \phi_j(\zeta) H(\zeta - \xi_i)\, \mathrm{d}\zeta, \tag{24}$$

where ξ_i is the coordinate of the ith node, and $H(\eta)$ the Heaviside step distribution, and $\phi_j(\zeta)$ the shape function associated with the node j.

If the shape functions $\phi_j(\zeta)$ are taken to be polynomials, the integrals in the foregoing equations decompose into binomial integrals that can be integrated analytically. In order to keep the algebra to a minimum, we selected linear interpolating functions as shown in Fig. 3. We will show that this selection is good enough for practical purposes.

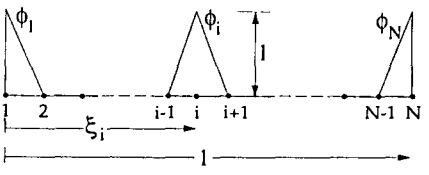

Fig. 3. Shape functions used in the numerical method.

3.2. Method of solution

In previous works [7, 8, 9] the method of solution used to solve (22) was an incremental and iterative Newton-Raphson. At present, direct iteration is used solving for the new value g_i from the previous value g_i^{pre} from the equation

$$L_{ij}g_j = F^*(R^* U_{ij} g_i^{\text{pre}}), \quad i, j = 1, 2, \ldots, N. \tag{25}$$

Since L_{ij} is lower triangular, each iteration involves forward substitution only, and is extremely fast. No convergence problems have been detected so far.

This algorithm has been implemented into a QuickBASIC program for Apple Macintosh. The program incorporates automatic search of the critical point (where $w(0) = w_c$), and at each increment, determines K_{IN}, ΔA_∞ and the stress and crack opening profiles over a user-selectable zone containing the cohesive region.

3.3. Error analysis

To estimate the degree of accuracy of the computations, various meshes have been used. Equi-spaced meshes with 2, 5, 10, 20, 40, 60 and 100 elements were analyzed.

The results showed that for a given variable the relative error increases with the size of the fracture zone. The maximum error thus corresponds to the critical situation. Of a number of variables (CTOD, K_{IN}, ΔA_∞) the relative error was greater for CTOD, so we use this variable to illustrate the dependence of the error on the element size.

Focusing on the linear softening ($F^*(w^*) = 1 - w^*/2$), Fig. 4 shows the evolution of the relative error on the prediction of the CTOD for $R = 0.7 l_{ch}$ (close to the critical value $R_c = 0.7312 l_{ch}$). From the figure it is clear that the convergence is quadratic and that the error is very low for as few elements as 5 (less than 0.3 percent). The extrapolated relative error for 100 elements is completely negligible: 33 parts per million.

The prediction of the stress and crack opening profiles is also excellent. Figure 5 compares the profiles in the critical situation computed using 100 elements, with the nodal values computed using 5 elements. The coincidence is very good for any practical purpose, and one may conclude that the numerical procedure is robust and accurate.

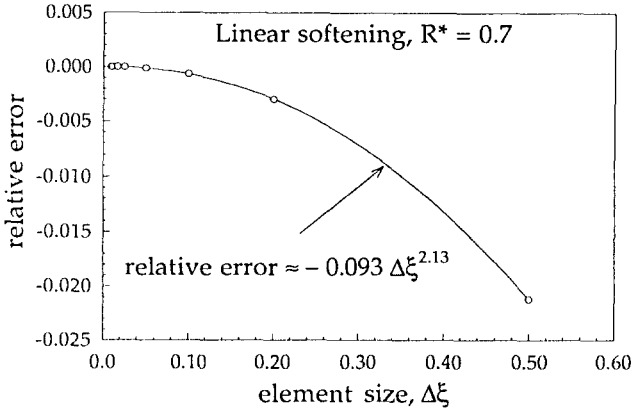

Fig. 4. Relative error of computed CTOD versus element size.

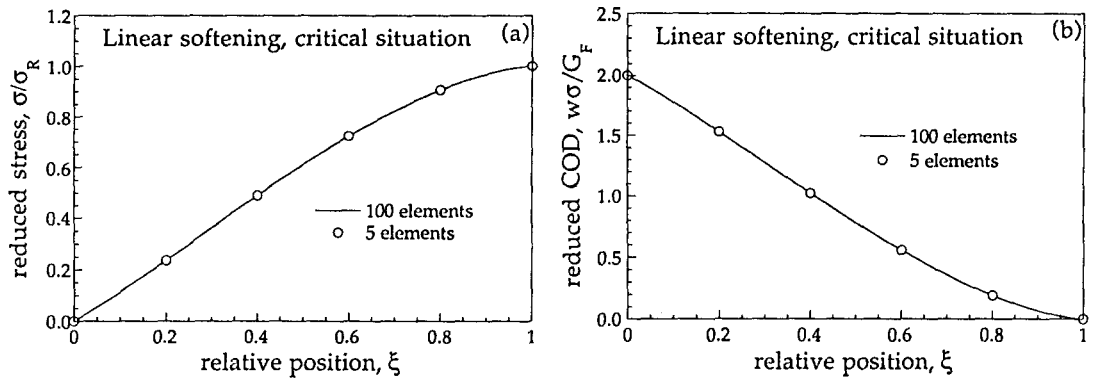

Fig. 5. Comparison of the profiles computed using a 100-element mesh (full line) and a 5-element mesh (open symbols). (a) Stress profiles. (b) Crack opening profiles.

4. Influence of the softening curve for large sizes

For large sizes it is possible to find some general trends depending on the material softening function; the shape of the stress and displacement functions near the crack tip are influenced by the kind of softening. The specimen compliance, a far field property, is also dependent on the softening function through the equivalent crack extension ΔA_∞. All these properties, and some others discussed below, will help in ascertaining the suitability of different softening models when analyzing experimental results.

4.1. Material softening curves

The analysis will be based on the following uniparametric family of softening curves

$$\begin{aligned} F^*(w^*) &= (1 + A)\,e^{-Bw^*} - A \quad \text{for} \quad 0 < w^* < w_c^*, \\ F^*(w^*) &= 0 \qquad\qquad\qquad\quad \text{for} \quad w^* \geqslant w_c^*, \end{aligned} \tag{26}$$

where

$$B = 1 - A \ln \frac{1 + A}{A} \tag{27}$$

and

$$w_c^* = \frac{1 - B}{AB}. \tag{28}$$

This family has the theoretical advantage of including as particular limiting cases the Dugdale model ($w_c^* = 1$), the straight line softening ($w_c^* = 2$) and the exponential softening ($w_c^* = \infty$). Moreover, the shape of the curves for w_c^* in the range 5 to 8 displays a marked similitude to the

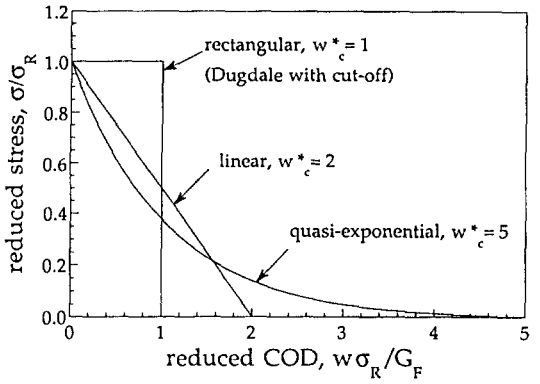

Fig. 6. Softening curves.

experimentally determined curves for concrete and cementitious materials. Figure 6 shows the shape of the curves for some selected values of the critical crack opening w_c^*.

The density function, in the zeroth order approximation, $k^*(\zeta)$ was computed for three different softening functions. The solution for the rectangular (Dugdale) model, was obtained analytically in previous work [7, 8] with the following result

$$k^*(\zeta) = \frac{1}{\pi}\zeta^{-1/2} \quad \text{or} \quad g(\zeta) = \frac{1}{\pi}. \tag{29}$$

For the other cases the density functions were obtained using the numerical methods described in the previous section.

A family of $g(\zeta)$ curves for several values of the cohesive zone R^*, corresponding to a material with linear softening is shown in Fig. 7a. The same results for a material exhibiting a quasi-exponential softening with $w_c^* = 5$, are depicted in Fig. 7b.

4.2. *Evolution of K_{IN} and of stress and crack opening profiles*

Once $g(\zeta)$ – and so also $k^*(\zeta)$ – are known, the nominal stress intensity factor K_{IN} and stress and displacement fields are computed respectively from expressions (12), (13) and (14).

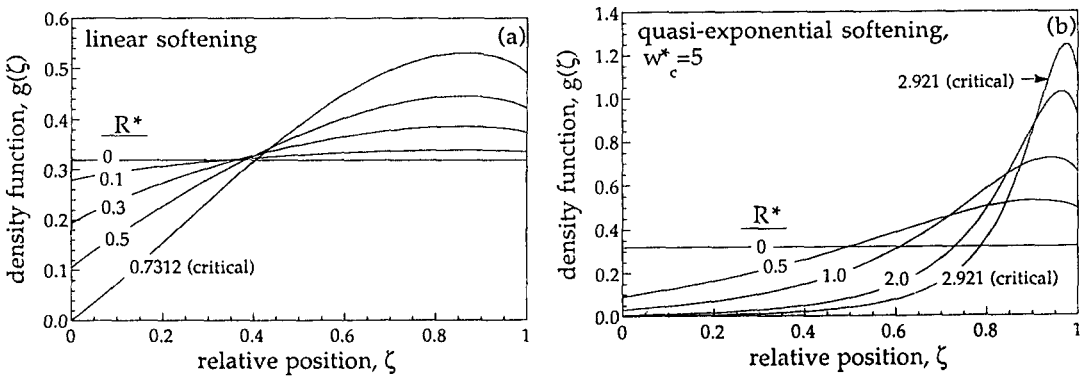

Fig. 7. Evolution of $g(\zeta)$ with R^*. (a) For linear softening. (b) For a quasi-exponential softening with $w_c^* = 5$.

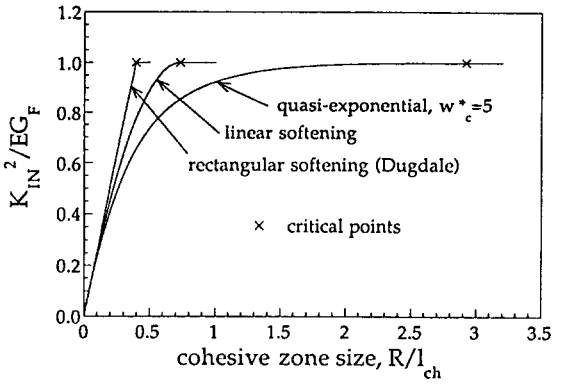

Fig. 8. Evolution of the nominal stress intensity factor with the size of the cohesive zone for various softening curves.

Figure 8 shows the evolution of the nominal stress intensity factor versus the cohesive crack extension for three softening curves: rectangular, linear and quasi-exponential with $w_c^* = 5$. The curves show that for small loads ($K_{IN}^2 < 0.2E'G_F$) the responses are very close. However, when the load approaches the peak, the sizes of the fracture zone become much larger for the materials with longer softening tails. In particular, the critical cohesive zone size is very different: $R_c^* = \frac{1}{8}\pi$ for rectangular softening, $R_c^* = 0.731$ for linear softening, and $R_c^* = 2.92$ for quasi-exponential (with $w_c^* = 5$). This strong dependence has also been observed by Smith, who used a combination of power laws for the critical distribution of crack openings along the cohesive zone to investigate the dependence of R_c^* on w_c^*. He proposed the approximate relationship (11)

$$\begin{aligned} R_c^* &\approx 0.4 w_c^* \quad \text{for} \quad w_c^* \leqslant 4, \\ R_c^* &\approx 0.1 w_c^{*2} \quad \text{for} \quad w_c^* \geqslant 4, \end{aligned} \tag{30}$$

which do capture the main trend of the results.

As a main conclusion of the foregoing, R_c^* is strongly dependent on the shape of the softening curve, particularly on the critical crack opening. Therefore, one may state that *if the critical cohesive zone length R_c^* can be measured, a good hint about the shape of the softening curve may be obtained.*

Figure 9a shows the *stress profiles*, for a material with linear softening, corresponding to various values of the cohesive zone length R^*. Figure 9b shows the same results for a material with quasi-exponential softening with $w_c^* = 5$.

When $R^* > R_c^*$, the cohesive zone travels in a self-similar way, at this level of approximation where very large sizes are considered (note that in this context, very large sizes imply very large distances from the cohesive zone to any outer surface of the body). From (13), it can be shown that these stresses are continuous at the tip of the cohesive zone ($\zeta, \xi = 1$), but that its derivative is discontinuous. For the chosen family of softening functions, with finite slope at the start of softening, the stress distribution at the left of the cohesive crack tip has a horizontal tangent, while at the right of this point the slope is $-\infty$. This behavior is depicted in Figs. 9a and 9b.

The *displacement profiles*, near the cohesive zone, are sketched in Fig. 10 for linear and quasi-exponential softening. The profiles correspond to different R^* values.

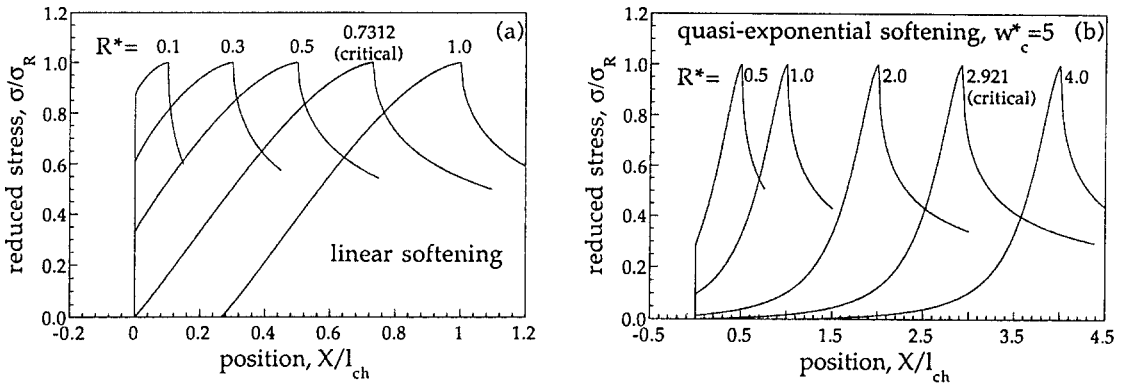

Fig. 9. Evolution of stress profiles with R^*. (a) For linear softening. (b) For a quasi-exponential softening with $w_c^* = 5$.

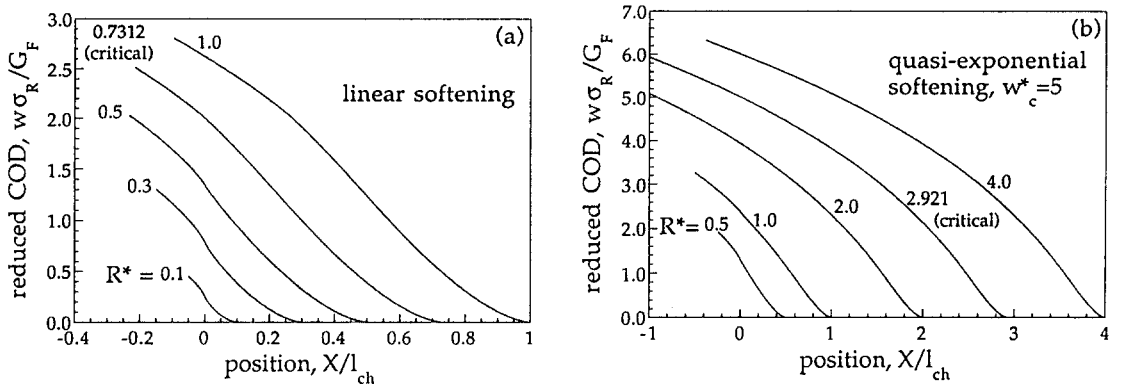

Fig. 10. Evolution of crack opening profiles with R^*. (a) For linear softening. (b) For a quasi-exponential softening with $w_c^* = 5$.

Cohesive crack displacements near the end of the process zone are not like those for elastic cracks which display vertical tangents and behave as $(1 - \xi)^{1/2}$. Instead, they display horizontal tangents and behave as $(1 - \xi)^{3/2}$ as is well known. The result obtained in [8] was

$$w^*(\xi) = \tfrac{16}{3} R^* k^*(1)(1 - \xi)^{3/2} + 0[(1 - \xi)^{3/2}]. \tag{31}$$

At the initial crack tip, the crack opening displacement is obtained by taking the limit of (14) when ξ approaches 0, i.e.

$$\mathrm{CTOD}^* = 8R^* \int_0^1 \zeta^{1/2} k^*(\zeta)\, \mathrm{d}\zeta = 8R^* \int_0^1 g(\zeta)\, \mathrm{d}\zeta. \tag{32}$$

Due to the singularity in $k^*(\zeta)$ the derivative of the crack opening displays a logarithmic singularity at the initial crack tip, and this singularity exists for any softening function until the CTOD reaches the critical crack opening value. This behavior is hard to see in the figures because it is very localized. However, the strong inflection it produces is clear in the profiles corresponding to small cohesive zones ($R^* \leqslant 0.3$) in Figs. 10a and 10b.

To grasp some information about the softening behavior (linear type or quasi-exponential, for example) of a cohesive material, a look at the displacements near the crack tip may throw some light, because displacements are dependent on the shape of the softening function, as depicted in Fig. 11 for the same cohesive zone extent. This kind of information can, in principle, be extracted from interferometric measurements, as reported for example by the research groups of S.P. Shah [12, 13], H. Horii [14] and A.S. Kobayashi [15]. However, the differences are quite small, and it may be extremely difficult in practice to get enough resolution to discriminate experimentally between the profiles shown in Fig. 11.

4.3. Equivalent crack extension

As pointed out in Section 2.4, the stress and displacement fields *far from the cohesive zone*, can be approximated by the corresponding far fields of an equivalent elastic crack of length $A_0 + \Delta A_\infty$. The equivalent crack extension ΔA_∞ is given by (15) together with (16). Figure 12 shows the computed evolution of the equivalent crack extension as the cohesive zone increases for various softening behaviors. From this figure it can be realized that the relation between ΔA^*_∞ and R^* is scarcely influenced by the softening behavior. Only the situation of the critical points (coinciding also with the peak) is strongly dependent on the particular softening. This means again that if the critical point can be experimentally detected, and the cohesive zone size measured, this would provide a good hint to ascertain the type of softening function.

It is interesting to compare the computed *critical* effective crack extension with its lower bound given by (17). Figure 13 shows that the computed results (open circles) lie very close to the lower bound, so that with a good approximation

$$\Delta A^*_{\infty c} \approx \frac{\pi}{32} w^{*2}_c. \tag{33}$$

This is a conclusion similar to that obtained by Smith using two-step, piece-wise rectangular softening functions [10], as Fig. 13 also shows as open squares (the results displayed correspond to two-step softenings such that the center of gravity of the area enclosed by the curve and the axes has an abscissa equal to w_{ch}).

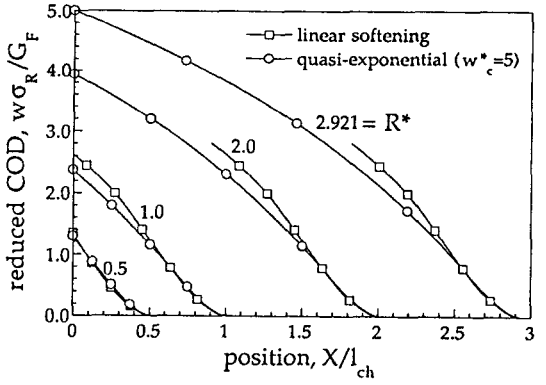

Fig. 11. Comparison of crack opening profiles for a linear softening and for a quasi-exponential softening with $w^*_c = 5$.

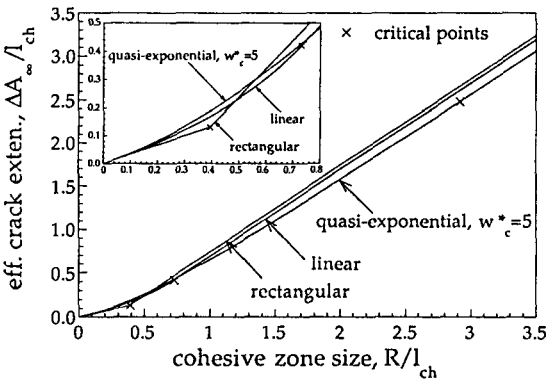

Fig. 12. Evolution of the equivalent crack extension with the cohesive zone length for various softening curves.

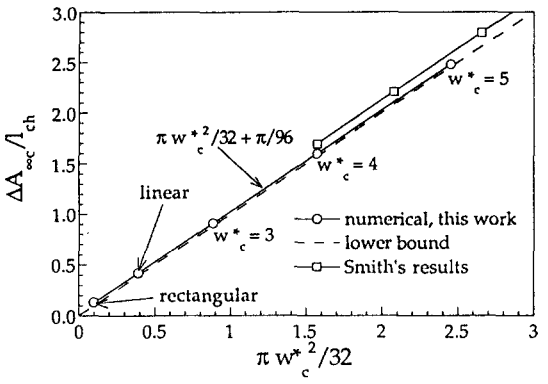

Fig. 13. Dependence of the critical effective crack extension on the critical crack opening w_c^*. Open circles correspond to our computations and open squares to Smith's analytical results for two-step softening.

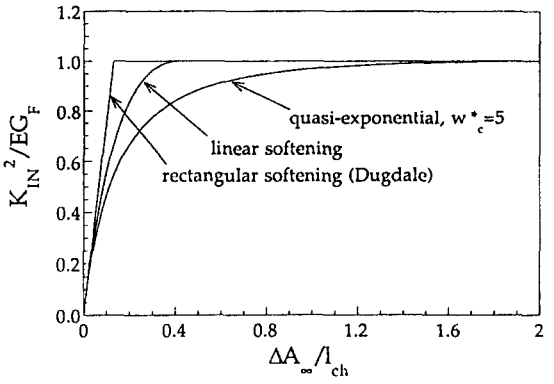

Fig. 14. Nominal stress intensity factor versus effective crack extension, expressed as $\mathscr{R}$-curves.

According to these results, in the cases where the size of the specimen is large enough for the asymptotic approximation to hold, the value of $\Delta A_{\infty c}$ may be inferred from the compliance at the peak, and an estimate made of the critical crack opening displacement w_c^* by means of (33).

Since the remote far-fields of the actual cohesive specimen coincide with those for an equivalent elastic crack of length $A_0 + \Delta A_\infty$ (up to first order), this correspondence was called far-field equivalence within a wider discussion of the various possible forms of equivalences [16, 17]. The associate $\mathscr{R}$-ΔA curve is the same for all far field equivalences and it is geometry and size independent, which is obvious if one uses the parametric equations (with parameter R^*) following from the basic relation $\mathscr{R} = J_R = K_{IN}^2/E'$, and (12), (15) and (16):

$$\frac{\mathscr{R}}{G_F} = 2\pi R^* \left[\int_0^1 k^*(\zeta; R^*)\, \mathrm{d}\zeta \right]^2, \tag{34}$$

$$\frac{\Delta A_\infty}{l_{ch}} = R^* \frac{\int_0^1 \zeta k^*(\zeta; R^*)\, \mathrm{d}\zeta}{\int_0^1 k^*(\zeta; R^*)\, \mathrm{d}\zeta}, \tag{35}$$

where the dependence of $k^*(\zeta)$ on R^* has been made explicit.

This result validates the use of a single $\mathscr{R}$-ΔA curve for design whenever $R/D \ll 1$, and shows that the $\mathscr{R}$-curve depends only on the softening function. Numerical results for $\mathscr{R}/G_F$ versus $\Delta A_\infty/l_{ch}$ are shown in Fig. 14 for various softening curves ($w_c^* = 1, 2$ and 5). From these curves it is apparent that for small values of ΔA_∞ the behavior is nearly the same for all softening curves, so that a Dugdale model may be used to describe the first stages of cracking. This is obviously not the case when the load approaches the critical point, since according to (33), $\Delta A_{\infty c}$ increases quadratically with w_c^*.

5. Implementation of the asymptotic concepts

5.1. When is a size a large size?

Throughout this paper, the sentence *for large enough sizes* was used to assure that the conditions for applicability of the asymptotic approximation were fulfilled. In practice, what one wants to know is the minimum required size for a sample of a cohesive material to be treated by linear elastic fracture mechanics, within some acceptable error. In particular one may require that the peak load corresponds to LEFM predictions within ε, i.e.

$$\frac{|K_{\mathrm{INmax}} - \sqrt{E'G_F}|}{\sqrt{E'G_F}} \leqslant \varepsilon. \tag{36}$$

If ε is small, we may take the first order size effect equation (20) as very close to the actual behavior, and find D_ε, the minimum size required to comply with (36). Neglecting second order terms in $1/\varepsilon$, the result is

$$D_\varepsilon^* = \frac{1}{\varepsilon}\frac{\beta_{01}}{\beta_{00}}\Delta A_{\infty c}^*, \tag{37}$$

which shows that the required size is inversely proportional to the accepted error. The proportionality coefficient decomposes into two factors. The first one, β_{01}/β_{00} is purely geometric and is fixed for a given specimen shape and relative initial crack depth. The second one, $\Delta A_{\infty c}^*$ is in fact a material property depending only on the shape of the softening curve, more specifically on the critical crack opening w_c^*: the longer the tail of the softening curve, the larger the size required for a given error.

To get an idea of the physical sizes involved, let us apply the above equation to various materials for an allowed 5 percent error, and a single edge notched beam in three point bending with a notch-to-depth ratio $A_0/D = 0.5$, where D is the beam depth. For such a geometry $\beta_{01}/\beta_{00} \approx 3$ (obtained from the analytical shape factor for the stress intensity factor given by Tada et al. [18]). Considering, furthermore, a quasi-exponential softening with $w_c^* \approx 5$ for which $\Delta A_{\infty c}^* \approx 2.5$ the required size turns out to be

$$D_{5\%} \approx 150 l_{ch}. \tag{38}$$

For an ordinary concrete we may take $G_F \approx 100$ N/m, $\sigma_R \approx 3$ MPa, and $E' \approx 30$ GPa, which give a characteristic length $l_{ch} \approx 0.33$ m. Therefore the required beam depth for 5 percent accuracy in peak load estimates becomes about 50 m. We may conclude that in most, if not all, practical experimental situations for ordinary concrete we are very far from the linear elastic fracture mechanics approach.

If we repeat these procedures for alumina (Al_2O_3) with $G_F \approx 55$ N/m, $\sigma_R \approx 220$ MPa, $E' \approx 280$ GPa, we find $l_{ch} \approx 0.32$ mm, and $D_{5\%}$ is about 48 mm, a reasonable size for laboratory testing.

Remark that the length of the softening tail (i.e. w_c^*) plays a paramount role in determining the required size of the specimen. If the classical approximation using rectangular softening is used,

the sizes are smaller by a factor of 20. However, experiments tend to show that the softening tails are quite long in quasi-brittle materials. In particular, values of w_c^* as large as 12 have been measured for concrete [19]. For alumina, w_c values of about 1/4 of the grain size, corresponding to values of w_c^* of 3–5, have been reported [6].

5.2. *Simplified computations for large sizes*

Even in the large size limit where the asymptotic expansion may be truncated to order zero, the only way to obtain reliable information of the behavior of the fields at or close to the cohesive zone is by numerical methods, such as those described in Section 3. However, if remote fields are all that is needed, the first order effective crack extension theorem may be invoked and the fields determined from a classical $\mathscr{R}$-ΔA formulation, using the $\mathscr{R}$-curves discussed in Section 4.3 and depicted in Fig. 14. From such an analysis, values such as compliances, remotely applied loads, remote crack profiles and path-independent integrals may be obtained.

It may be reasonably argued that the determination of the $\mathscr{R}$-curve for a given softening still requires the complete numerical solution. This is true. But the use of the asymptotic $\mathscr{R}$-curve may still be helpful because of its ease of use in graphical reasoning. And at any rate, the asymptotic $\mathscr{R}$-curve for a given softening shape is unique and has to be computed only once for this particular softening.

It is possible to use an approximate $\mathscr{R}$-curve having an explicit (closed-form) expression in terms of the CTOD. In the end, this approximation consists of substituting the effective crack extension ΔA_∞ by its lower bound (17), which has a closed form expression in terms of the CTOD. More formally, this substitution stems from a special equivalence, called the J-CTOD equivalence [17] in which the load and the crack extension of an equivalent elastic specimen are computed in such a way that the J-integral and the CTOD are identical to those in the actual specimen. The effective crack extension in the J-CTOD equivalence is denoted as $\Delta A^{J-\mathrm{CTOD}}$, and the parametric equations (with parameter CTOD) of the $\mathscr{R}$-curve are found [17] as

$$\frac{\mathscr{R}}{G_F} = W_F^*(\mathrm{CTOD}^*), \tag{39}$$

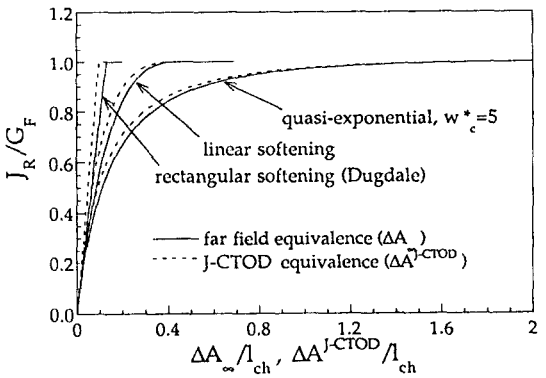

Fig. 15. Comparison of the true far field $\mathscr{R}$-curves and the approximate $\mathscr{R}$-curves obtained from the J-CTOD equivalence.

$$\frac{\Delta A^{J\text{-CTOD}}}{l_{ch}} = \frac{\pi}{32} \frac{\text{CTOD}^{*2}}{W_F^*(\text{CTOD}^*)}. \tag{40}$$

Figure 15 compares the true far-field $\mathscr{R}$-curves with those obtained from the foregoing approximation. It is obvious that they are very close, particularly for long-tailed softenings. Therefore, the J-CTOD equivalence may be a useful short-cut to get fast and fairly accurate solutions for the remote fields and related variables.

Acknowledgments

This work was supported by Dirección General de Investigación Científica y Técnica (DGICYT) Spain, under grants No. PB 90-0276 and MAT 92-0031. The work has also benefitted from discussion in this general problem area with Prof. E. Smith, Manchester University-UMIST, U.K., via the British-Spanish Joint Research Programme (Acciones Integradas).

References

1. G.J. Barenblatt, *Advances in Applied Mechanics* 7 (1962) 55–125.
2. D.S. Dugdale, *Journal of Mechanics and Physics of Solids* 8 (1960) 100–104.
3. A. Hillerborg, M. Modeer and P.E. Petersson, *Cement and Concrete Research* 6 (1976) 773–782.
4. A. Hillerborg, *Materials and Structures* (1985) 291–296.
5. R.F. Cook, C.F. Fairbanks, B.R. Lawn and Y.W. Mai, *Journal of Materials Research* 2 (1987) 345–356.
6. R.W. Steimbretch, A. Reichl and W. Schaarwächter, *Journal of the American Ceramics Society* 73 (1990) 2009–2015.
7. J. Planas and M. Elices, *Anales de Mecánica de la Fractura* 3 (1986) 219–227.
8. J. Planas and M. Elices, *International Journal of Fracture* 55 (1991) 153–177.
9. Ibid, 51 (1991) 139–157.
10. E. Smith, The elastically equivalent softening zone size for an elastic-softening material: II. A simple piece-wise softening law, submitted for publication.
11. E. Smith, When can we apply LEFM principles to elastic softening materials?, submitted for publication.
12. A. Castro-Montero, S.P. Shah and R.A. Miller, *Journal of Engineering Mechanics*, ASCE 116 (1990) 2463–2484.
13. R.A. Miller, A. Castro-Montero and S.P. Shah, *Journal of the American Ceramics Society* 74 (1991) 130–138.
14. H. Horii and T. Ichinomiya, *International Journal of Fracture* 51 (1991) 19–29.
15. J.J. Du, A.S. Kobayashi and N.M. Hawkins, *Engineering Fracture Mechanics* 35 (1990) 15–27.
16. M. Elices and J. Planas, *International Journal of Fracture* 61 (1993) 159–172.
17. J. Planas, M. Elices and G. Ruiz, *International Journal of Fracture* 61 (1993) 231–246.
18. H. Tada, P. Paris and G. Irwin, *The Stress Analysis of Cracks Handbook*, Del Research Corp. (1985).
19. K. Rokugo, M, Iwasa, T. Suzuki and W. Koyagani, in *Fracture Toughness and Fracture Energy, Test Methods for Concrete and Rock*, Mihashi et al. (eds.) Balkema, Rotterdam (1989) 153–163.